Int. J. Electrochem. Sci., 15 **(2020)** 1 – 15, doi: 10.20964/2020.01.39

International Journal of
ELECTROCHEMICAL
SCIENCE
www.electrochemsci.org

Corrosion Inhibition Performance of Coconut Leaf Extract as a Green Corrosion Inhibitor for X65 Steel in Hydrochloric Acid Solution

Siyi Chen[*], *Bin Zhu, Xing Liang*

College of Chemistry and Chemical Engineering, Zunyi Normal University, Zunyi 563002, PR China.
[*]E-mail: chensiyijiayou@163.com

Received: 3 September 2019 / *Accepted:* 30 October 2019 / *Published:* 30 November 2019

In this paper, coconut leaf extract was extracted with absolute ethanol. The corrosion inhibition performance of coconut extract on X65 steel in the corrosive medium of HCl was studied using electrochemical ways, surface morphology analysis, and theoretical calculations. Experimental data of potentiodynamic polarization curves indicated that coconut extract is a mixed-type corrosion inhibitor. Surface morphology analysis test results showed that coconut leaf extract can effectively inhibit the corrosion of X65 steel. The adsorption of coconut leaf extract on the X65 steel surface conforms to the Langmuir single layer adsorption. Quantum chemical calculations and molecular dynamics simulations can effectively demonstrate that coconut leaf extracts exhibit excellent corrosion inhibition performance.

Keyword: Coconut leaf extract; X65 steel; Corrosion inhibitor; Langmuir adsorption model; Quantum chemical calculations; Molecular dynamics simulations

1. INTRODUCTION

X65 steel is widely used in the transportation of natural gas due to its good corrosion protection capability [1, 2]. Unfortunately, during prolonged service, X65 steel is clearly attacked by corrosive ions in natural gas. In order to effectively observe the corrosion of the surface of X65 steel, pickling becomes very important. Hydrochloric acid is one of the most frequently used pickling solutions [3-5]. Although pickling can effectively remove the corrosive medium on the X65 steel surface, it also corrodes the X65 steel substrate to some extent. Therefore, the addition of corrosion inhibitors to the pickling solution has become one of the simplest and most effective methods to inhibit the corrosion of metal [6-10]. Adding corrosion inhibitor can not only effectively inhibit the corrosion of hydrochloric acid on the X65 steel substrate, but also effectively reduce the use of hydrochloric acid. Therefore, the research and development of corrosion inhibitors has important industrial application value.

Generally, organic corrosion inhibitors contain conjugated functional groups and contain heteroatoms such as oxygen (O), sulfur (S), nitrogen (N), phosphorus (P), etc [11-14]. These heteroatoms provide a lone pair of electrons that can bond to the empty orbitals of the metal. Although organic corrosion inhibitors can effectively inhibit metal corrosion, many organic corrosion inhibitors can pose certain threats to humans and the ecological environment [15, 16]. Therefore, research on high-efficiency and non-toxic corrosion inhibitors has become a hot spot for corrosion workers.

Wang et al. [17] researched Ficus tikoua leaves extract as an eco-friendly corrosion inhibitor for carbon steel in HCl media. The electrochemical results reveal that the extract inhibitors act as a mixed-type with an inhibition efficiency up to 95.8% at 298 K. Qiang et al.[18] researched Ginkgo leaf extract as an eco-friendly corrosion inhibitor of X70 steel in HCl solution. The inhibition efficiency exceeded 90% in the presence of 200 mg/L GLE at all of the tested temperatures. Ramezanzadeh et al.[19] researched corrosion inhibition of mild steel in 1 M HCl solution by ethanolic extract of eco-friendly Mangifera indica (mango) leaves. Results revealed that with increasing inhibitor concentration and immersion time the inhibition efficiency increased and reached the maximum value of 92% after 24 h in the presence of 1000 ppm inhibitor. In our work, it can be found that the coconut leaf extract has a concentration of 400 mg/L at 298 K. The corrosion inhibition efficiency is up to 94%.

In this work, coconut leaf extract (CLE) was studied as a highly effective environmentally friendly corrosion inhibitor. It is well known that coconut leaves grow under tropical temperatures. It grows fast and has a wide range of sources. Therefore, it is an ideal raw material as a corrosion inhibitor. We extracted the coconut leaves by pure extraction. The corrosion inhibition performance of the obtained coconut leaf extract was experimentally and theoretically studied. The experimental results show that the coconut leaf extract exhibits excellent corrosion inhibition performance.

2. EXPERIMENTAL METHOD

2.1. Preparation of coconut leaf extract

The coconut leaves were collected in Hainan, China, cleaned with ultrapure water, dried for 60 h at 343 K, and then ground to powder. The 40 g coconut leaves powder were refluxed in 75% alcohol at 363 K for 6 h. Then, the solution was concentrated in a rotary evaporator, and then dried in a vacuum dry oven for 48 h. Put the obtained 5 g of coconut leaves powder into the desiccator for use. The coconut leaf extract was characterized by Fourier transform infrared spectroscopy (Nicolet iS50) with the range of 400−4000 cm^{-1}.

2.2. Preparation of electrode materials and solutions

The chemical composition of X65 steel is shown in Table 1. The size of 1×1×1 cm^3 X65 steel samples used for work electrode. The other sides of the X65 steel was sealed with epoxy resin leaving only a working area of 1×1 cm^2. 1 M hydrochloric acid solution was prepared with ultrapure water and concentrated hydrochloric acid. The extracted coconut leaf extract was formulated into the test solution of 50, 100, 200, 300, and 400 mg/L.

2.3. Electrochemical tests

All electrochemical experiments in this paper were performed on the CHI604D electrochemical workstation in a traditional three-electrode system. In this three-electrode system, X65 steel was used as the working electrode, platinum electrode was used as the counter electrode, and saturated calomel electrode was used as the reference electrode. X65 steel needs to be sanded in 400 to 2000 # sandpapers before conducting electrochemical experiments. After polishing, the surface of X65 steel is cleaned with ultrapure water. Finally, dry in anhydrous ethanol for use. The electrochemical test consists of three parts. Firstly, the measurement of the open circuit potential was carried out, and the time was selected to be 1800 seconds to ensure that the X65 steel reaches a steady state. The second step was to conduct an electrochemical impedance spectroscopy test. The disturbance signal was a 10 mV peak-to-peak sinusoidal wave in the frequency range of 100 kHz – 0.01 Hz. Impedance data is fitted in a Zsimpwin software. Finally, the potentiodynamic polarization curves test was performed. The range of polarization was Eocp ± 250 mV. The scanning rate was 0.167 mV/s.

Table 1. Chemical composition of X65 steel.

Elements	Fe	Mn	Si	Cr	C	Nb	Al
Proportion	97.894 %	1.64 %	0.17 %	0.16 %	0.06 %	0.041 %	0.035%

2.4. Surface topography analysis

After 4 h immersion in 1 mol/L hydrochloric acid without and with 400 mg/L CLE, the X65 steel samples were rinsed with deionized water, and dried under 298 K. The X65 steel morphologies of the 4 h immersion samples were tested through FE-SEM (JEOL-JSM-7800F). The X65 steel morphologies of the 2 h immersion samples with same procedure were tested through AFM (MFP-3D-BIO) with tapping mode.

2.5. Calculation details

The chemical constitutions of the coconut leaf extract were tested by the infrared spectroscopy test. We used Materials Studio (MS) software to calculate the properties of the main constitutions using DFT. Geometry Optimization as the computational tasks, GGA and PBE as the Functional, Energy was 1×10^{-5} Ha, Max force was 0.002 Ha/Å, and Max displacement was 0.005 Å, respectively.

The adsorption of coconut leaf extract on the Fe(110) surface was calculated with the forcite module in MS software. Firstly, we create a Fe(110) model with a size of 20 Å × 20 Å × 40 Å. Then this vacuum layer was filled with 300 H_2O molecules and a coconut leaf extract molecule. The calculated task was Dynamics, the Ensemble was NVT, the Time step was1fs, and the total calculation time was 2000 ps. Forcefield was COMPASS, Electrostatic and van der Waals were ewald.

3. RESULTS AND DISCUSSION

3.1. FTIR analysis

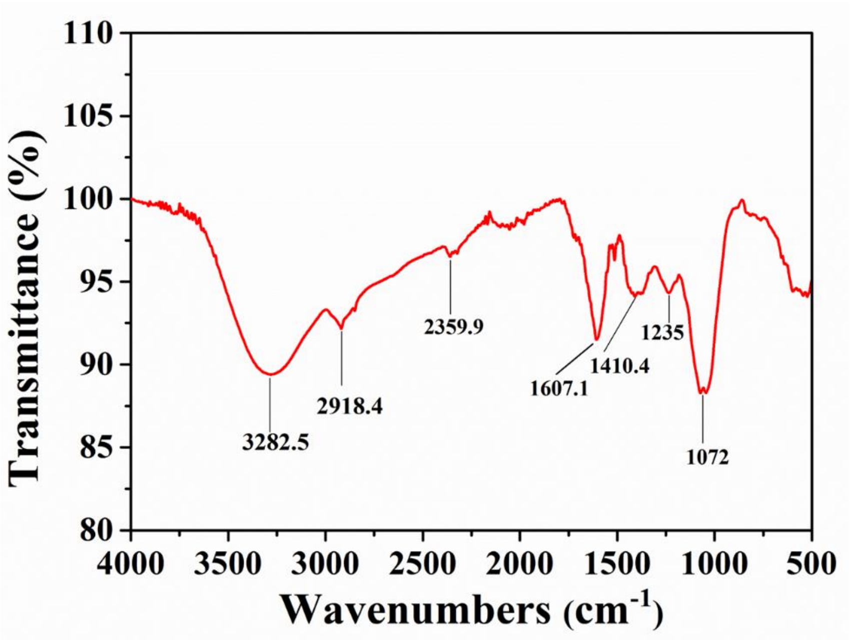

Figure 1. FTIR spectra of CLE.

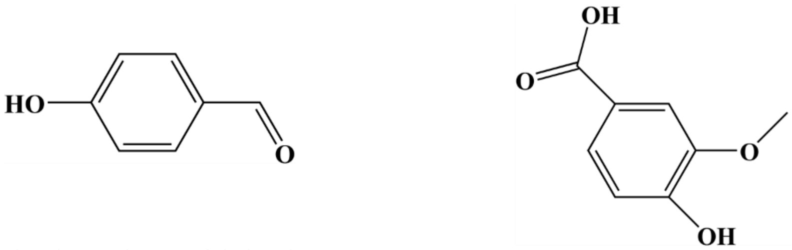

4-hydroxybenzaldehyde 4-hydroxy-3-methoxybenzoic acid

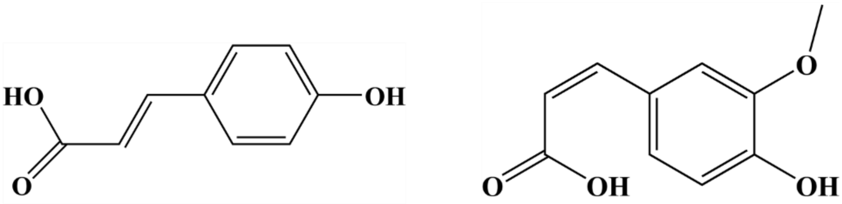

3-(4-hydroxy-phenyl)-acrylic acid 3-(4-hydroxy-3-methoxyphenyl)acrylic acid

Figure 2. The main molecular formulas of CLE.

The FTIR spectroscopy of CLE is shown in Figure 1. The broad band at 3282.5 cm^{-1} is related to O–H stretching. The peak located at 2918.4 cm^{-1} is attributed to C–H stretching vibration, and that at 1607 cm^{-1} to C=O. The absorption band at 1410.4 cm^{-1} is attributed to the framework vibration of aromatic ring. The C–H bending in $-CH_3$ is found to be at 1235 cm^{-1}. The absorption band at 1072 cm^{-1}, which is attributed to the C–O stretching vibration [18]. By analyzing the results of infrared spectroscopy, it can be found that CLE contains a large amount of oxygen-containing functional groups.

According to the related references of CLE, it can be judged based on the four organic substances. They are 4-hydroxybenzaldehyde (HDD), 4-hydroxy-3-methoxybenzoic acid (HDA), 3-(4-hydroxy-phenyl)-acrylic acid (HPA) and 3-(4-hydroxy-3-methoxyphenyl)acrylic acid (HMA). Their molecular formulas are shown in Figure 2.

3.2. Potentiodynamic polarization curves analysis

Figure 3 shows the potentiodynamic polarization curves at different concentrations of CLE at 298 K. It can be found that the corrosion current density decreases significantly with the increase of CLE concentration. This indicates that CLE can effectively inhibit the corrosion of X65 steel in hydrochloric acid solution. All of the cathodic polarization curves in Figure 3 showed a parallel trend, indicating that the adsorption of CLE on the surface of the X65 steel did not change the reaction mechanism of the cathode. The slope of the anode branching curves are clearly changed, indicating that the mechanism of the anodic reaction has changed. That is to say, the adsorption of coconut leaf extract on the X65 steel surface can effectively inhibit the dissolution of Fe^{2+}.

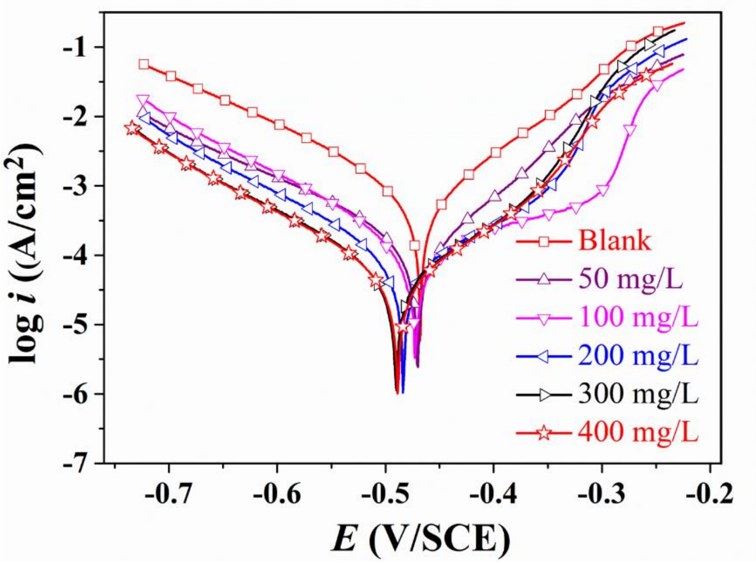

Figure 3. The potentiodynamic polarization curves for X79 steel in 1 M HCl at different concentrations of CLE at 298 K.

The Tafel extrapolation method was used to obtain the corrosion current density, the corrosion potential, and the slope of the anode and cathode. The parameters obtained are listed in Table 2. The corrosion current density is obtained by the following formula [20-23]:

$$\eta(\%) = \frac{i_{corr,0} - i_{corr}}{i_{corr,0}} \times 100 \qquad (1)$$

where $i_{corr,\,0}$ and i_{corr} indicate the corrosion current density of without and with coconut leaf extract, respectively. It can be found that the corrosion potential value is −0.468 V when no CLE is added. After the addition of CLE, the corrosion potential moved significantly toward the cathode, indicating that CLE inhibited the cathode more than the anode. The maximum corrosion potential change was 32 mV, significantly less than 85 mV, indicating that CLE is a mixed-type corrosion inhibitor [24]. When the concentration of CLE is 400 mg/L, the inhibition efficiency at this time is as high as 94.1%.This shows that CLE can exhibit excellent anti-corrosion performance.

Table 2. Polarization curve parameters for X79 steel in 1 M HCl at different concentrations of CLE at 298 K.

C (mg/L)	E_{corr}(V/SCE)	I_{corr}(μA cm^{-2})	β_c(mV dec^{-1})	β_a(mV dec^{-1})	η (%)
Blank	–0.468	595.8	–102	88	—
CLE					
50	–0.471	118.5	–96	98	80.1
100	–0.473	91.7	–98	104	84.6
200	–0.484	67.3	–102	99	88.7
300	–0.490	45.8	–105	97	92.3
400	–0.489	35.1	–99	104	94.1

3.3. Electrochemical impedance spectroscopy

Figure 4 shows Niqust plot and Bode plot at different CLE concentrations for X65 steel in 1 M HCl at 298 K. As shown in Figure 4(a), as the concentration of CLE increases, the radius of the capacitive loop increases significantly. This indicates that the charge transfer resistance is increased due to the adsorption of CLE, which has a significant inhibitory effect on the corrosion of X65 steel. The shapes of Niqust plot have not changed significantly, indicating that the adsorption of CLE on the surface of X65 steel has little change in its reaction mechanism.

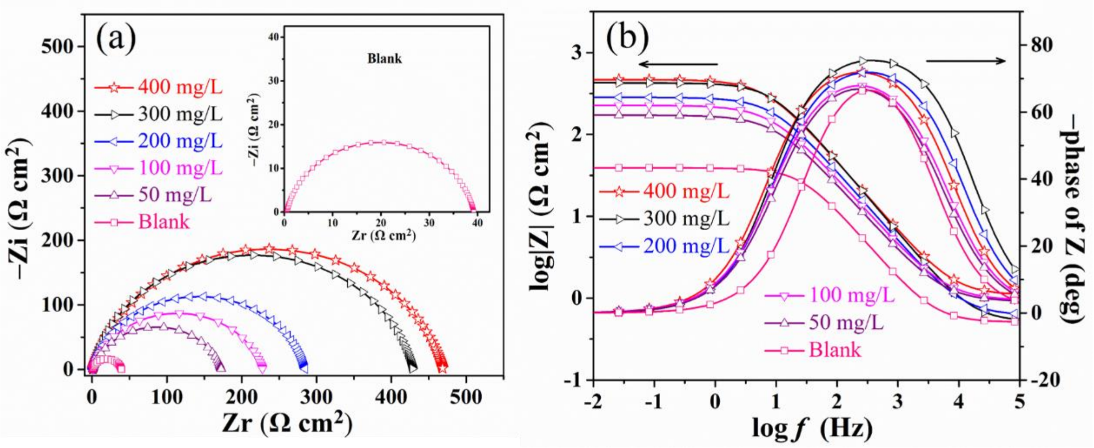

Figure 4. The (a) Niqust plot and (b) Bode plot at different CLE concentrations for X65 steel in 1 M HCl at 298 K.

As shown in Fig. 4b, in the low frequency region, the capacitive reactance modulus is significantly increased by an order of magnitude. In addition, in the intermediate frequency region, the slope of the impedance modulus can be found to be close to 1. It indicates that CLE has a capacitance property in X65 steel [25]. In addition, it can be seen that only one peak appears in the phase angle, indicating that CLE only produces a time constant when adsorbed on the surface of X65 steel.

In order to understand the electrochemical impedance spectroscopy in depth, we used the equivalent circuit diagram (Figure 5) to fit the EIS data. The fitted experimental data is listed in Table 3. The calculation formula of corrosion inhibition efficiency is as follow [26]:

$$\eta(\%) = \frac{R_{ct} - R_{ct,0}}{R_{ct}} \times 100 \qquad (2)$$

where R_{ct} and $R_{ct,\,0}$ represent charge transfer resistance with and without CLE. In Table 3, the electric double layer capacitance (C_{dl}) can be calculated by the following formulas [27, 28]:

$$Z_{CPE} = \frac{1}{Y_0(j\omega)^n} \qquad (3)$$

$$C = Y_0(\omega)^{n-1} = Y_0(2\pi f_{Z_{im-Max}})^{n-1} \qquad (4)$$

As shown in Figure 3, the values of C_{dl} decrease significantly as the concentration of CLE increases, because CLE replaces the water molecules on the surface of X65 steel. Which is explained by the following formula [29, 30]:

$$C_{dl} = \frac{\varepsilon^0 \varepsilon}{d} S \qquad (5)$$

According to formula 5, it is found that the more the value of C_{dl} decreases, indicating that the more water molecules CLE replaces the surface of X65 steel, the denser the protective film is formed. In addition, it is worth mentioning that the value of the deviation index n is significantly close to 1. As the concentration of CLE increases, this indicates that CLE forms a dense protective film on the surface of X65 steel.

Table 3. Impedance spectrum data

C (mg/L)	R_s (Ω cm^2)	$Y_0 \times 10^{-6}$ (S s^n cm^{-2})	*n*	C_{dl} (μF cm^{-2})	R_{ct} (Ω cm^2)	η (%)
Blank	0.87	182.5	0.87	180.7	38.7	-
CLE						
50	0.47	95.1	0.91	80.9	171.8	77.5
100	0.32	76.3	0.93	64.1	226.9	82.9
200	0.59	62.3	0.94	56.3	284.3	86.4
300	0.38	59.2	0.96	45.1	427.7	90.9
400	0.68	48.9	0.98	32.7	467.7	91.7

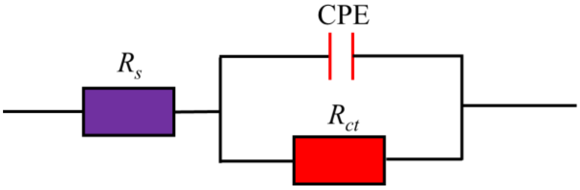

Figure 5. Equivalent circuit diagram for fitting impedance spectrum data.

3.4. Adsorption isotherm model research

In order to study the specific information of CLE adsorption on the surface of X65 steel. We used different isothermal adsorption models to fit the polarization curve data. The fitted linear regression coefficients indicate that the adsorption of CLE on the surface of X65 steel conforms to the Langmuir adsorption isotherm model. The fitted data is listed in Figure 6.

The Langmuir adsorption isotherm is as follow [31-35]:

$$\frac{C}{\theta}=\frac{1}{K_{ads}}+C \qquad (6)$$

where C represents the concentration of CLE. η indicates the surface coverage. K_{ads} is the adsorption equilibrium constant. In order to explore the type of adsorption of CLE on the X65 steel surface. We used the following formula to calculate the Gibbs free energy (ΔG^0_{ads}) [18]:

$$K_{ads}=\frac{1}{1000}\exp(-\frac{\Delta G^0_{ads}}{RT}) \qquad (7)$$

The calculated K_{ads} and ΔG^0_{ads} values are listed in Figure 6. The value of ΔG^0_{ads} is related to the types of adsorption. When the ΔG^0_{ads} value is greater than –20 kJ/mol, it indicates that the corrosion inhibitor molecules are physically adsorbed on the metal surface.

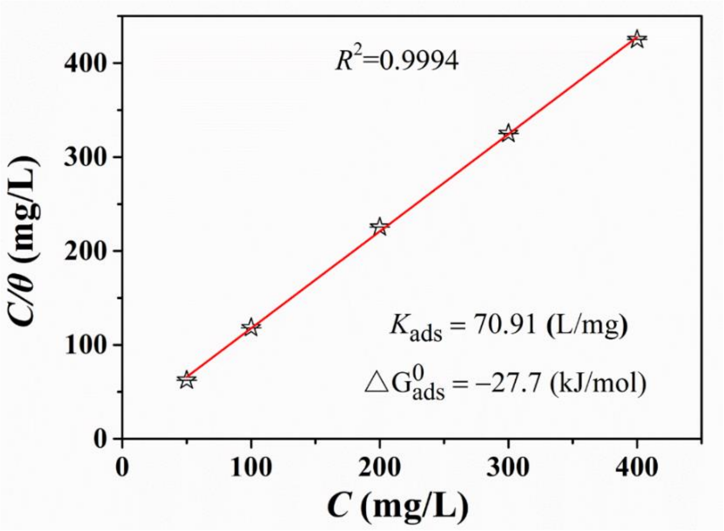

Figure 6. Langmuir adsorption isotherm (data from figure 3 and Table 2).

When the value of ΔG^{0}_{ads} is less than −40 kJ/mol, it indicates that the corrosion inhibitor molecules are chemically adsorbed on the metal surface. When the value of ΔG^{0}_{ads} is between −20 and −40 kJ/mol, it indicates that the corrosion inhibitor molecules have a physical and chemical adsorption interaction on the metal surface [31, 36, 37]. Therefore, it can be judged that the adsorption of CLE on the surface of X65 steel belongs to physical and chemical adsorption.

3.5. SEM analysis

Figure 7 shows the surface morphology of X65 steel under different conditions. As shown in Figure 7(a), the surface of the X65 steel has been polished to leave a lot of scratches. Figure 7 (b) is the surface topography of X65 steel immersed in 1 M hydrochloric acid with 400 mg / L of CLE for 4 hours at 298 K. It can be found that the entire X65 steel surface is relatively flat. Figure 7 (c) is the surface topography of X65 steel immersed in 1 M hydrochloric acid for 4 hours at 298 K without CLE. It can be found that the entire X65 steel has been severely corroded. Corrosion holes are very obvious. By comparing Figures 7(b) and (c), it can be shown that CLE can exhibit excellent corrosion inhibition performance.

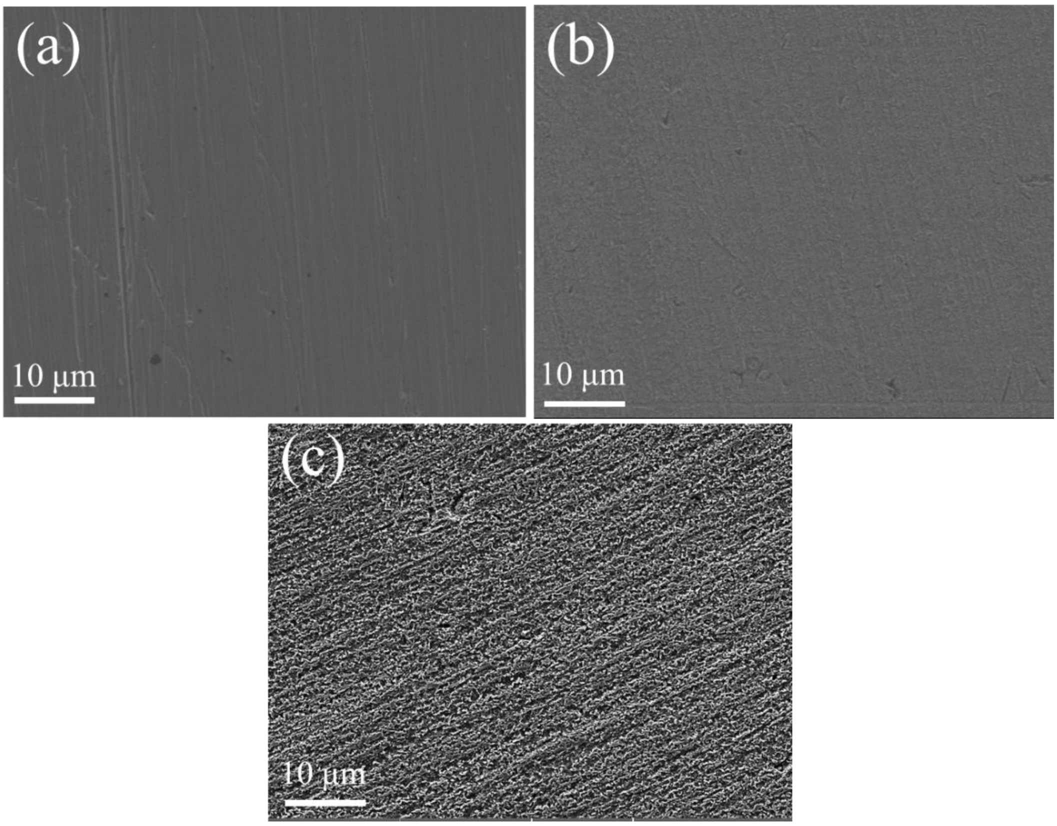

Figure 7. The surface morphology of X65 steel under different conditions: (a) Freshly polished surface, (b) Steel surface with 400 mg/L CLE soaked in hydrochloric acid for 4 hours at 298 K, (c) Steel surface without CLE soaked in hydrochloric acid for 4 hours at 298 K.

3.6. AFM analysis

Figure 8 shows the 3D surface morphology of X65 steel under different conditions. Figure 9 is the 2D contour map of the surface of X65 steel under different conditions. Figure 8 (a) is the 3D surface topography of polished X65 steel. After the X65 steel is just ground, the roughness of the entire surface is 8.6 nm. Figure 8 (b) is the 3D surface topography of X65 steel immersed in 1 M hydrochloric acid with 400 mg / L of CLE for 2 hours at 298 K. The roughness of the entire X65 steel surface is 10.8 nm.

Figure 8 (c) is the 3D surface topography of X65 steel immersed in 1 M hydrochloric acid for 2 hours at 298 K without CLE. The roughness of the entire X65 steel surface has exceeded 40 nm. AFM test results and SEM are highly consistent.

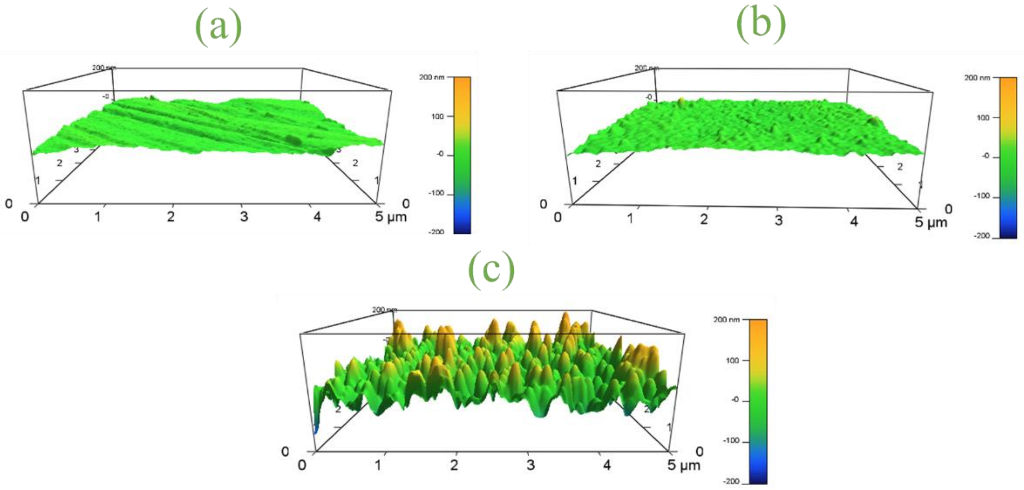

Figure 8. The 3D surface morphology of X65 steel under different conditions: (a) Freshly polished surface, (b) Steel surface with 400mg/L CLE soaked in hydrochloric acid for 2 hours at 298 K, (c) Steel surface without CLE soaked in hydrochloric acid for 2 hours at 298 K.

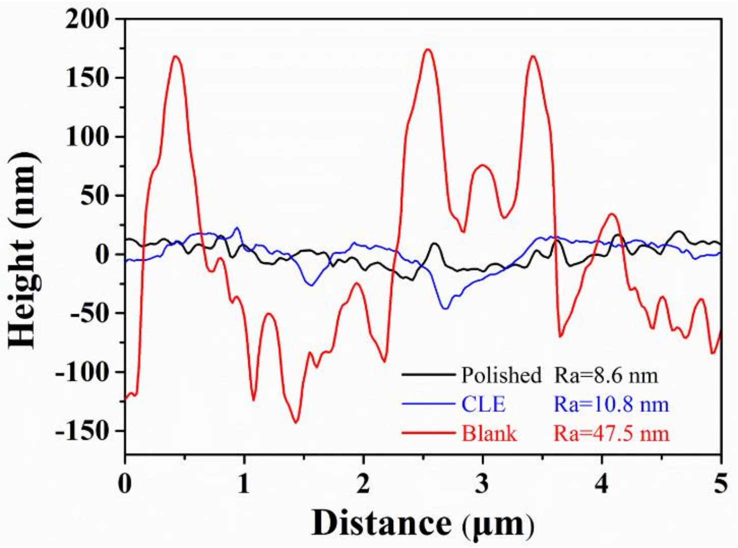

Figure 9. The 2D contour map of X65 steel surface under different conditions for 2 hours at 298 K.

3.7. Quantum chemical calculation analysis

The quantum chemical calculation plays an important role in the research and development of new corrosion inhibitors. It can effectively predict the corrosion inhibition performance of the corrosion inhibitor by the nature of the corrosion inhibitor molecule, thereby saving a lot of material and financial resources. In this work, we calculated important quantitative parameters of coconut leaf extract by MS software.

Figure 10 presents the optimized configuration of four substances in coconut leaf extract, frontier molecular orbital distribution. According to the frontier molecular orbital theory, the HOMO orbit involves the ability of molecules to give electrons. The LUMO orbital is related to the electronic ability of the molecule [38]. As shown in Figure 10, the electron cloud densities of HDD, HPA, HDA and HMA molecules are distributed almost entirely throughout the molecules. This indicates that the four molecules are more likely to adsorb in parallel on the surface of the X65 steel.

Figure 11 presents the electrostatic potential map of four substances in coconut leaf extract. Nucleophilic and electrophilic properties of a molecule represented by red and blue regions, respectively [39, 40]. It can be clearly found that the red region is mainly distributed on the oxygen-containing functional group. Therefore, these oxygen-containing functional groups can form a chemical bond with the surface of the X65 steel and adsorb on the surface of the X65 steel. Thus, CLE can exhibit excellent corrosion inhibition performance.

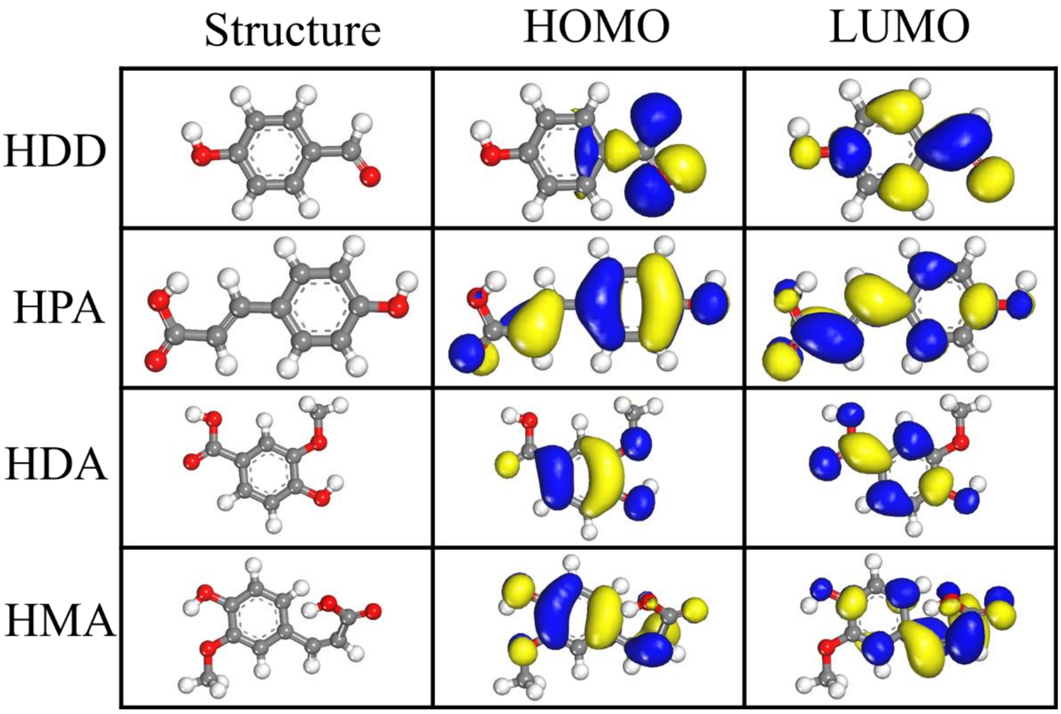

Figure 10. The optimized configuration of four substances in coconut leaf extract, frontier molecular orbital distribution.

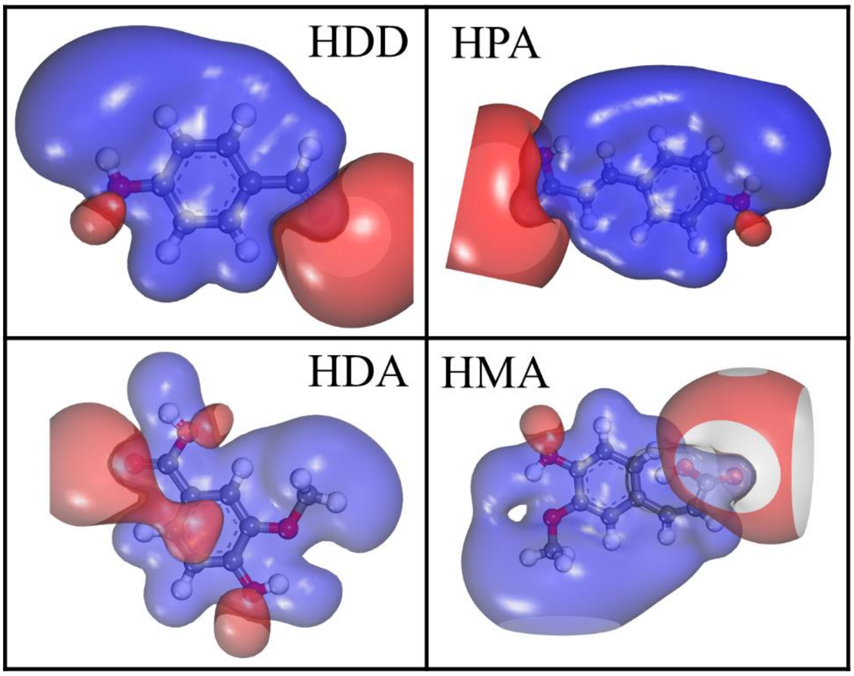

Figure 11. The electrostatic potential map of four substances in coconut leaf extract.

Figure 12 shows the values of dipole moment and energy gap of four coconut leaf extracts. In general, the smaller the energy gap value, the better the corrosion inhibitor properties of the corrosion inhibitor molecules [31]. As shown in Figure 12(a), the order of their gap values is HMA < HPA < HDD < HDA. Therefore, their order of corrosion inhibition ability for X65 steel in hydrochloric acid is HDA < HDD < HPA < HMA.

Dipole moment is also an important parameter to assessment corrosion inhibition performance. Most researchers believe that the larger the dipole value, the better the adsorption of corrosion inhibitor on the metal surface. Therefore, as shown in Figure 12(b), HMA has the greatest contribution to the corrosion inhibition performance of X65 steel in hydrochloric acid.

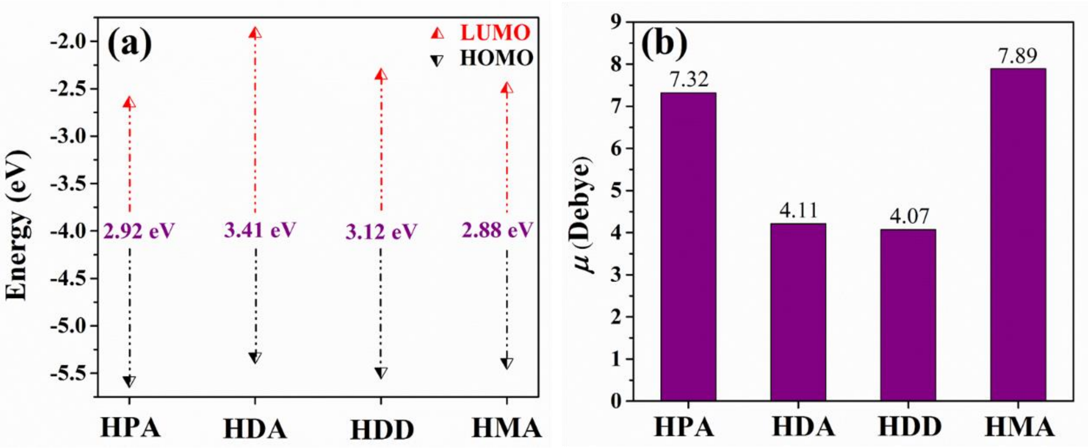

Figure 12. Quantum chemical parameters (the values of energy gap and dipole moment) of HPA, HAD, HDD, and HMA in CLE.

3.8. Molecular dynamics simulation analysis

Molecular dynamics simulation can effectively study the adsorption configuration of the metal surface of the corrosion inhibitor molecule. Therefore, it has been widely used in the field of research of corrosion inhibitors. Figure 13 shows the adsorption configuration of four corrosion inhibitor molecules on the surface of X65 steel. It can be found that HPA, HAD, HDD, and HMA molecules can be adsorbed on the Fe(110) surface in parallel. This is consistent with the results obtained in the molecular orbital analysis section. The binding energy of HPA, HAD, HDD, and HMA molecules on the surface of Fe(110) is obtained by the following formula [41]:

$$E_{binding} = -E_{\mathrm{int}\,eract} \qquad (8)$$

$$E_{\mathrm{int}\,eract} = E_{tot} - (E_{subs} + E_{inh}) \qquad (9)$$

where E_{tot} stands for the total energy of the whole simulation system, E_{sub} stands for the total energy of 300 H_2O molecules and Fe(110) substrate, and E_{inh} stands for the energy of researched molecule. The binding energy of HPA, HAD, HDD, and HMA molecules on the surface of Fe(110) are 213.1 kJ/mol, 178.9 kJ/mol, 165.3 kJ/mol, and 382.9 kJ/mol, respectively. The order of their combined energy is HMA > HPA > HDA > HDD. This is consistent with the quantitative calculation results.

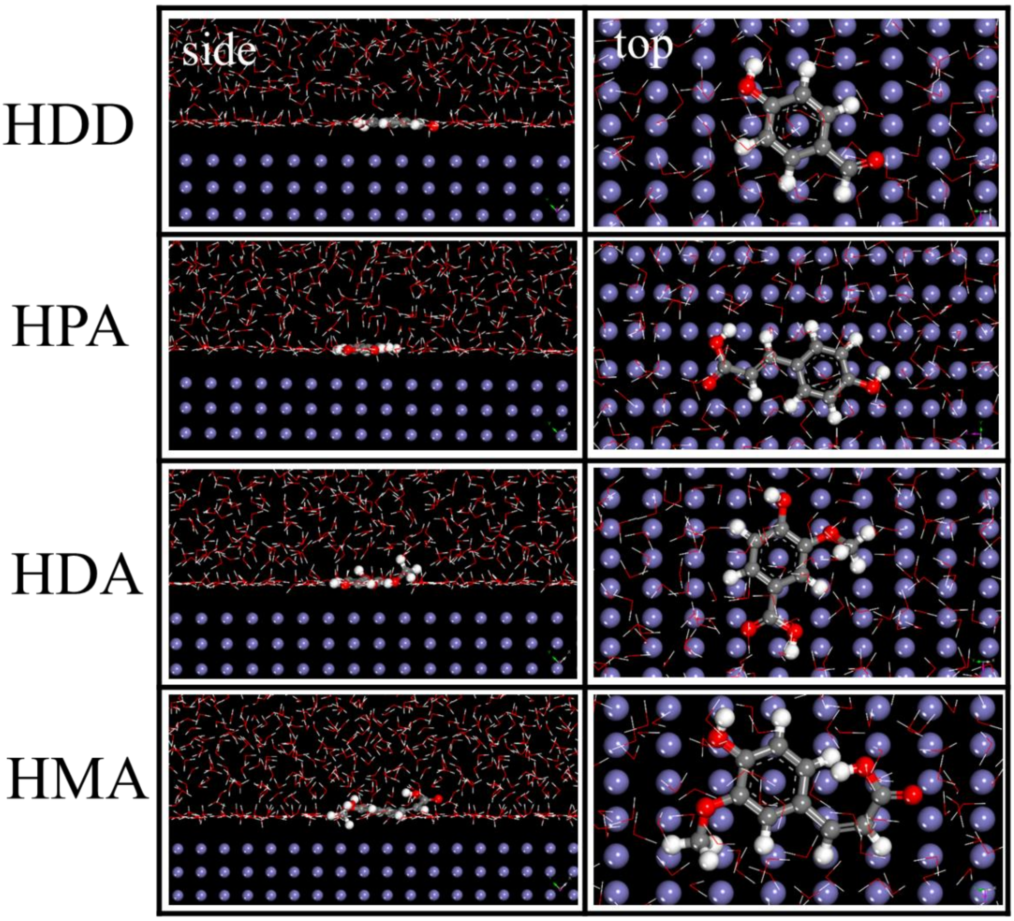

Figure 13. Adsorption configurations of four corrosion inhibitor molecules on the X65 steel surface.

4. CONCLUSIONS

Electrochemical test results show that coconut extract shows excellent corrosion inhibition performance and is a mixed corrosion inhibitor. The adsorption of coconut extract on the surface of the X65 steel creates a relaxation process. Surface morphology analysis and electrochemical experiment results are consistent. The adsorption of coconut leaf extract on the surface of X65 steel conforms to Langmuir's single layer adsorption. Quantum chemical calculations and molecular dynamics simulations have proven that four major substances exhibit excellent corrosion inhibition performance.

References

1. A. Singh, K.R. Ansari, J. Haque, P. Dohare, H. Lgaz, R. Salghi, and M.A. Quraishi, *J. Taiwan Inst. Chem. E.*, 82 (2018) 233.
2. A. Biswas, P. Mourya, D. Mondal, S. Pal, and G. Udayabhanu, *J. Mol. Liq.*, 251 (2018) 470.
3. F. El-Hajjaji, M. Messali, A. Aljuhani, M.R. Aouad, B. Hammouti, M.E. Belghiti, D.S. Chauhan, and M.A. Quraishi, *J. Mol. Liq.*, 249 (2018) 997.
4. E. Alibakhshi, M. Ramezanzadeh, G. Bahlakeh, B. Ramezanzadeh, M. Mahdavian, and M. Motamedi, *J. Mol. Liq.*, 255 (2018) 185.
5. P.E. Alvarez, M.V. Fiori-Bimbi, A. Neske, and S.A. Brandán, C.A. Gervasi, *J. Ind. Eng. Chem.*, 58 (2018) 92.
6. N.D. Nam, P.V. Hien, N.T. Hoai, and V.T.H. Thu, *J. Taiwan Inst. Chem. E.*, 91 (2018) 556.
7. M. Ramezanzadeh, Z. Sanaei, G. Bahlakeh, and B. Ramezanzadeh, *J. Mol. Liq.*, 256 (2018) 67.
8. M.R. Zahra Sanaei, Ghasem Bahlakeh, and Bahram Ramezanzadeh, *J. Ind. Eng. Chem.*, 69 (2019) 18.
9. R.N. Leili Rassoulia, and Mohammad Mahdavain, *J. Ind. Eng. Chem.*, 66 (2018) 221.
10. F. El-Hajjaji, M. Messali, M.V. Martinez de Yuso, E. Rodriguez-Castellon, S. Almutairi, T.J. Bandosz, and M. Algarra, *J. Colloid Interf. Sci.*, 541 (2019) 418.
11. M. M. Antonijevic, and M. B. Petrovic, *Int. J. Electrochem. Sci.*, 3 (2008) 1
12. B. Tan, S. Zhang, H. Liu, Y. Qiang, W. Li, L. Guo, and S. Chen, *J. Taiwan Inst. Chem. E.* 102 (2019) 424.
13. Y. Qiang, S. Zhang, and L. Wang, *Appl. Surf. Sci.*, 492 (2019) 228.
14. J. Zhang, L. Zhang, and G. Tao, *J. Mol. Liq.*, 272 (2018) 369.
15. L.L. Liao, S. Mo, H.Q. Luo, and N.B. Li, *J. Colloid Interf. Sci.*, 520 (2018) 41.
16. X. Zhang, and B. Tan, *Int. J. Electrochem. Sci.*, 13 (2018) 11388.
17. Q. Wang, B. Tan, H. Bao, Y. Xie, Y. Mou, P. Li, D. Chen, Y. Shi, X. Li, and W. Yang, Bioelectrochemistry 128 (2019) 49.
18. Y. Qiang, S. Fu, S. Zhang, S. Chen, and X. Zou, *Corros. Sci.*, 140 (2018) 111.
19. M. Ramezanzadeh, G. Bahlakeh, Z. Sanaei, and B. Ramezanzadeh, *Appl. Surf. Sci.*, 463 (2019) 1058.
20. Y. Qiang, S. Fu, S. Zhang, S. Chen, and X. Zou, *Corros. Sci.*, 140 (2018) 111.
21. M.B. Radovanović, and M.M. Antonijević, *J. Adhe. Sci. Technol.*, 31 (2016) 369.
22. N.K. Othman, S. Yahya, and M.C. Ismail, *J. Ind. Eng. Chem.*, 70 (2019) 299.
23. B.R. M. Motamedi, and M. Mahdavian, *J. Ind. Eng. Chem.*, 66 (2018) 116.
24. Y. Qiang, S. Zhang, S. Yan, X. Zou, and S. Chen, *Corros. Sci.*, 126 (2017) 295.
25. Y. Qiang, S. Zhang, L. Guo, X. Zheng, B. Xiang, and S. Chen, *Corros. Sci.*, 119 (2017) 68.
26. P. Kannan, T.S. Rao, N. Rajendran, *J. Colloid Interf. Sci.*, 512 (2018) 618.
27. B. Tan, S. Zhang, H. Liu, Y. Guo, Y. Qiang, W. Li, L. Guo, C. Xu, and S. Chen, *J. Colloid Interf. Sci.*, 538 (2019) 519.

28. M.M. Solomon, S.A. Umoren, M.A. Quraishi, and M. Salman, *J. Colloid Interf. Sci.*, 551 (2019) 47.
29. B. Tan, S. Zhang, Y. Qiang, L. Feng, C. Liao, Y. Xu, and S. Chen, *J. Mol. Liq.*, 248 (2017) 902.
30. S. Tao, and H. Huang, *Int. J. Electrochem. Sci.,* 14 (2019) 5435.
31. B. Tan, S. Zhang, Y. Qiang, L. Guo, L. Feng, C. Liao, Y. Xu, and S. Chen, *J. Colloid Interf. Sci.*, 526 (2018) 268.
32. Z.Z. Tasic, M.M. Antonijevic, M.B. Petrovic Mihajlovic, and M.B. Radovanovic, *J. Mol.Liq.*, 219 (2016) 463.
33. S. Chen, B. Xiang, S. Chen, X. Zou, Y. Zhou, and J. Hou, *Appl. Surf. Sci.*, 456 (2018) 25.
34. X. Li, S. Deng, T. Lin, X. Xie, and G. Du, *J. Taiwan Inst. Chem. E.*, 86 (2018) 252.
35. K. Zhang, W. Yang, B. Xu, Y. Chen, X. Yin, Y. Liu, and H. Zuo, *J. Colloid Interf. Sci.*, 517 (2018) 52.
36. A. Mishra, C. Verma, H. Lgaz, V. Srivastava, M.A. Quraishi, and E.E. Ebenso, *J. Mol. Liq.*, 251 (2018) 317.
37. P.R. Charitha B P, *J. Ind. Eng. Chem.,* 58 (2018) 357.
38. M. Abd El-Raouf, E.A. Khamis, M.T.H. Abou Kana, and N.A. Negm, *J. Mol. Liq.*, 255 (2018) 341.
39. B. Tan, S. Zhang, Y. Qiang, W. Li, H. Liu, C. Xu, and S. Chen, *J. Mol. Liq.*, 286 (2019) 110891.
40. Y. Qiang, S. Zhang, L. Guo, S. Xu, L. Feng, I.B. Obot, and S. Chen, *J. Clean. Prod.*, 152 (2017) 17.
41. B. Tan, S. Zhang, W. Li, X. Zuo, Y. Qiang, L. Xu, J. Hao, and S. Chen, *J. Ind. Eng. Chem.*, 77 (2019) 449.